Available online at www.sciencedirect.com
ScienceDirect
Trans. Nonferrous Met. Soc. China 33(2023) 889−901
Transactions of Nonferrous Metals Society of China
www.tnmsc.cn

New method and application of disturbance range prediction for caving method of metal ore

Ke-ping ZHOU[1], Liang LI[1], Yun LIN[1], Xin XIONG[1], Nian-ge YANG[1], Shu-lin CHEN[2]

1. School of Resources and Safety Engineering, Central South University, Changsha 410083, China;
2. Panzhihua Iron Mine, Panzhihua Iron and Steel Mining Co., Ltd., Panzhihua 617025, China

Received 28 November 2021; accepted 18 May 2022

Abstract: To quantify the disturbance range of the metal ore caving method, a new method to predict the disturbance range based on rock mechanics parameters is proposed. By combining the rock mechanics index with random medium theory, the prediction correction formula of the disturbance range is established. Based on disturbance equivalent centre and disturbance attenuation sphere, the two-dimensional safety criterion of mining disturbance in metal mines is derived. The new method is applied to 6 mines and the Jianshan Iron Mine, and the numerical simulation of the Jianshan Iron Mine by FLAC^{3D} model is performed. The posteriori error ratio between predicted value and measured value is 0.0357, and the multi-factor cross analysis shows that the relative error of this method to the result is only 0.078. It is found that the method has high prediction accuracy and does not significantly affect the security.

Key words: disturbance range; correction formula; two-dimensional safety criterion; numerical simulation; multi-factor cross analysis

1 Introduction

Large-scale mining under metal mines leads to uneven settlement of surface buildings, which results in huge losses. The advanced prediction of the mining disturbance range can reduce losses [1,2]. Existing mining disturbance subsidence research can be divided into four categories.

(1) Fitting of the settlement curve [3−5]. According to the subsidence status of the mine surface, a fitting curve that can explain the existing subsidence law is obtained by fitting, and the applicability of the fitting curve is proven to evaluate the subsidence damage degree of the mine.

(2) Application of modern technology in mining subsidence. Differential interferometric synthetic aperture radar technology and GPS technology have been widely studied in settlement measurements [6−12]. The application of FALC^{3D} in mining simulation makes the study of mine surface subsidence more intuitive.

(3) Prediction method based on mathematical theory. The subsidence prediction model is established based on Boltzmann−Knothe function, the grey model and Markov process, which provides different research perspectives to study the mining subsidence [13,14].

(4) Application of an intelligent algorithm in subsidence prediction. The rough set-BP neural network, cellular mechanism and group genetic algorithm are used to establish a subsidence prediction model, which provides the possibility for solving surface subsidence problems in special metal mines [15−17].

Based on the above research, although there are many studies on the surface subsidence of metal mines, there is no simple and applicable quantitative standard for the disturbance range of metal mines. Most studies obtain a static influence

Corresponding author: Yun LIN, Tel: +86-18373197457, E-mail: yunlin617@163.com
DOI: 10.1016/S1003-6326(23)66153-9
1003-6326/© 2023 The Nonferrous Metals Society of China. Published by Elsevier Ltd & Science Press

circle from the mining termination boundary, and few people consider the dynamic response of rock mechanics during excavation.

Since the essence of mining subsidence is the deformation and failure of rock and soil, a modified formula for the mining disturbance range is proposed by combining random medium theory with rock mechanics parameters. To compensate for the deficiency of the static prediction theory of mining subsidence, the concepts of the disturbance equivalent centre and disturbance attenuation sphere are proposed. Based on the perturbation equivalent centre and perturbation attenuation sphere, the two-dimensional criterion of perturbation safety for the metal ore caving method is derived. The safe movement angle of the Jianshan Iron Mine of China is studied through the new prediction model to optimize its mining resources. The disturbance ranges of six underground caving mines are predicted and compared with the measured values. The prediction accuracy of the new model is higher. To verify the influence of the new method on safety, a FLAC^{3D} simulation of the Jianshan excavation is performed. Finally, the prediction results of the new model and numerical simulation results are analyzed by the multi-factor cross analysis, which proves that the relative error caused by the new method can be ignored.

2 Corrected formula of disturbance distance and acquisition mode of correction factor

2.1 Correction of perturbation formula based on random medium theory

An empirical formula is proposed for the disturbance range of underground mining [18]:

$$r_z = \sqrt{4\pi A z} \tag{1}$$

$$A = \lim_{\substack{a\to 0\\ b\to 0}} \frac{a^2}{8b} \tag{2}$$

where r_z is the mining disturbance distance, m; A is the random medium walk coefficient, z is the height difference between the mining level and surface, m; a and b are the increments in the X-direction and Z-direction in the random medium walk model, respectively, m.

We substitute Formula (2) into Formula (1) to obtain the empirical formula of the disturbance range of underground mining based on the random walk model.

$$r_z = \lim_{\substack{a\to 0\\ b\to 0}} \sqrt{\frac{\pi a^2 z}{2b}} \tag{3}$$

Obviously, Formula (3) cannot be directly applied to metal mines. According to fractal geometry and approximate similarity theory, the loose ellipsoid of the mine is mined by the caving method to replace the small ball in the random swimming model [19,20]. There is a certain error between the micromotion model and the macrodrawing unit, so a disturbance prediction correction formula suitable for caving mining is proposed [21].

$$r_{\mathrm{d}} = k\sqrt{\frac{\pi H_{\mathrm{S}}^2 \left(H_{\mathrm{G}} - H_{\mathrm{KC}}\right)}{2R}} \tag{4}$$

where r_{d} is the modified disturbance radius of underground metal ore caving mining, m; R is the maximum radius of the discharge funnel, m; H_{S} is the height of the loose ellipsoid, m; H_{G} is the average elevation of the research object, m; H_{KC} is the elevation of the section being mined, m; k is the correction factor.

The random medium theory describes the exponential relationship between the surface micro settlement and the square of the X coordinate of the mining unit [22]. Similar to random medium theory, there is an exponential relationship between the disturbance correction coefficient and a certain factor. However, the displacement variable in the Z-direction is the focus of random medium theory. The proposed disturbance in this work is the direction where the weak surface of the rock and soil mass is the most prone to damage, and it has a certain angle with the Z-direction [23]. If the Z-direction is taken as the axial direction, then the maximum perturbation direction is the shear strain direction. Referring to the definition of the shear modulus, the correction coefficient is defined as follows [24]:

$$k = \frac{\mathrm{e}^{\mu}}{2(1+v)} \tag{5}$$

where v is Poisson ratio and μ is the correction factor. For rock and soil mass objects with various lithologies, μ is recommended to perform the weight estimation and obtain the correction factor

for the mining disturbance formula. The mechanical properties of ore and rock play an important role in surface collapse [25]. Therefore, this study obtains the disturbance correction factor based on the mechanics viewpoint.

2.2 Determination of simplified correction factor based on rock strength

In most of the existing prediction methods and models, the mining influence is mostly predicted from the perspective of geometry and pure mathematics, but the influence of rock mechanical properties on surface deformation cannot be ignored.

Upper plate progressive theory notes that once tensile failure occurs in the upper plate area of mining, the tension instability will increase with increasing mining depth, which results in new tensile fractures on the surface [12]. To fully consider the influence of the mechanical properties of the rock mass on the prediction of the disturbance distance, the modified formula is also optimized based on the principle of simple application. The disturbance correction factor is approximated by the ratio of the smaller value to the larger value in the mean value and the median value in the rock strength test, which is named as the median ratio.

Based on some viewpoints in the Hoek−Brown strength criterion and the upper panel asymptotic theory, the prediction formula of surface disturbance caused by caving mining is closely related to the uniaxial tensile and compressive strengths of the rock mass [26]. Therefore, these two strength errors are used to approximate the correction factor, i.e., the correction factor of the disturbance range can be characterized as

$$\mu=\frac{1}{2}\left[\frac{\min(X_{\mathrm{cz}},\bar{X}_{\mathrm{c}})}{\max(X_{\mathrm{cz}},\bar{X}_{\mathrm{c}})}+\frac{\min(X_{\mathrm{tz}},\bar{X}_{\mathrm{tc}})}{\max(X_{\mathrm{tz}},\bar{X}_{\mathrm{tc}})}\right] \tag{6}$$

where X_{cz} is the median of the uniaxial compressive strength of multiple samples; $\bar{X}_{\mathrm{c}}$ is the expected uniaxial compressive strength of a group of specimens; X_{tz} is the median uniaxial tensile strength of multiple specimens; $\bar{X}_{\mathrm{tc}}$ is the expected uniaxial tensile strength of a group of specimens.

2.3 Parameter adjustment of multi-boundary constraints in metal mines

In the actual production of metal mines, due to various forms of deposit occurrence and the level of mining technology and equipment, these restrictions are studied as boundary problems of disturbance distance prediction [27,28].

$$E_{\mathrm{f}}=\frac{\mathrm{e}^{\mu}}{2(1+\nu)}\sqrt{\frac{\pi H_{\mathrm{S}}^{2}\Delta H}{2R}}-r_{\mathrm{c}}+\sum_{i=1}^{n}\lambda_i[G_i(x,\ y,\ z,\ \mu,\ R,\ H_{\mathrm{S}},\ t,\ \sigma_1,\ \sigma_3,\ \phi)-A_i] \tag{7}$$

where E_{f} is the error function; ΔH is the elevation difference; r_{c} is the disturbance distance of measured surface subsidence, m; λ_i is Lagrange multiplier; G_i is the function in the function cluster of multivariate constraints; x, y, and z are the spatial coordinates and geometric fractal constraints; t is time, the failure of rock mass has rheology and creep, so time is also taken as the boundary constraint variable; σ_1 and σ_3 are the first and third principal stresses, respectively; ϕ is the internal friction angle; A_i is the value in the boundary domain.

When the error function takes the minimum value, it is most reasonable to take some values in the prediction formula. Therefore, partial derivatives can be obtained for each parameter from Formula (7):

$$\begin{cases}\dfrac{\partial(E_{\mathrm{f}})}{\partial\mu}=0, & \dfrac{\partial(E_{\mathrm{f}})}{\partial R}=0, & \dfrac{\partial(E_{\mathrm{f}})}{\partial H_S}=0\\ \dfrac{\partial(E_{\mathrm{f}})}{\partial x}=0, & \dfrac{\partial(E_{\mathrm{f}})}{\partial y}=0, & \dfrac{\partial(E_{\mathrm{f}})}{\partial z}=0\\ \dfrac{\partial(E_{\mathrm{f}})}{\partial t}=0, & \dfrac{\partial(E_{\mathrm{f}})}{\partial\sigma_1}=0, & \dfrac{\partial(E_{\mathrm{f}})}{\partial\sigma_3}=0\\ \dfrac{\partial(E_{\mathrm{f}})}{\partial\phi}=0, & \displaystyle\sum_{i=1}^{n}\frac{\partial(E_{\mathrm{f}})}{\partial\lambda_i}=0 & \end{cases} \tag{8}$$

By solving Formula (8), the corresponding parameters can be obtained to fine-tune the parameter values in Formula (4). Moreover, some useful boundary parameters can be obtained, which provides the basis for the ground pressure management of the mine and the reference for the efficient and coordinated convergence in time.

2.4 Dimension reduction and formula derivation of disturbance safety criterion

In this study, as long as the actual distance is greater than the disturbance radius, it indicates that underground mining has no effect (or is safe) on

highways, which is characterized as

$$r_s > r_d \tag{9}$$

where r_s is the sphere radius from the disturbance centre to the surface under different rock stratum movement angles.

To investigate the three-dimensional safety disturbance criterion from an analytical viewpoint, based on the premise that the same subsection is fully mined (the ore volume outside the security pillar) and the rock stratum is homogeneous and isotropic, an equivalent center that radiates the influence of mining in the form of a sphere is equivalent [29,30]. The influence surface of mining disturbance is called the disturbance attenuation sphere, i.e., the disturbance effect gradually decreases with increasing distance because the disturbance energy is firstly released on the ground closest to the equivalent disturbance center. According to the second law of thermodynamics, other energy radiated from the disturbance center has not been released, and there is a trend of energy diffusion to this position [31]. Therefore, the surface firstly affected by the disturbance attenuation sphere is the most prone to collapse failure and forms a collapse circle [32−35]. Based on these ideal conditions, the spatial geometric relationship of the three-dimensional criterion of Jianshan underground iron ore is shown in Fig. 1.

The rock types of the same mine generally show diverse characteristics, and the development of faults, joints and fissures greatly affects the study of rock movement angles. The heterogeneity of the rock mass also makes it difficult to study the rock movement angle, so the observed value is different from the real angle. In this study, it is assumed that the observed moving angle is representative of the entire rock mass, and the error between the observed moving angle and the actual moving angle was acceptable. Therefore, the time-dependent working condition function of the moving angle was introduced.

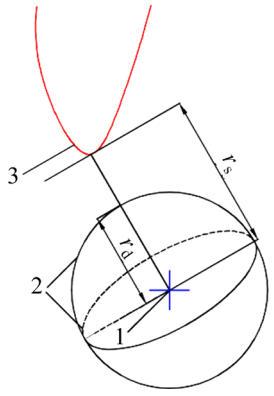

Fig. 1 Disturbance criterion of metal collapse method: 1−Equivalent disturbance center of excavation; 2− Energy attenuation sphere of excavation disturbance; 3− Disturbance boundary line

$$\theta(t) = \sum_{n=0}^{\infty} \frac{\theta^n(t)}{n!}(t - t_0) \tag{10}$$

where $\theta(t)$ is the working condition function of the moving angle, n is the a sequence variable, and t_0 is the initial time node with significant surface disturbance.

To be more applicable, the Taylor series second-order expansion of Formula (10) was obtained:

$$\theta(t) = \theta(t_0) + \theta'(t_0)(t - t_0) + \frac{1}{2}\theta''(t_0)(t - t_0)^2 \tag{11}$$

Formula (9) can be more specifically expressed as

$$\left(\frac{\Delta H}{\tan\theta(t)} + L_{KC}\right)^2 + (\Delta H)^2 > r_d^2 \tag{12}$$

where L_{KC} is the distance from the boundary of the security pillar that is vertically near the road side to the stope center.

The disturbance of underground caving mining radiates around in the form of an energy attenuation sphere, so L_{KC} can be expressed as

$$L_{KC} = \frac{1}{2}(\delta_k - \delta_z) \tag{13}$$

where δ_k is the total thickness of the ore body, which is a constant for a mine with a preliminary development scheme, and δ_z is the average thickness of the left security pillar.

Substituting Formula (13) into Formula (12) yields

$$\left(\frac{\Delta H}{\tan\theta(t)} + \frac{\delta_k - \delta_z}{2}\right)^2 + (\Delta H)^2 > r_d^2 \tag{14}$$

There are two unknown parameters δ_k and ΔH ($\theta(t)$ is known) in Formula (14), which creates some difficulties for engineering applications. However, in-depth research has found a relationship between these two variables. A conservatively estimated rock movement angle $\delta_{\theta^\wedge}$ links the two variable parameters, and Formula (14) is transformed into:

$$\left(\frac{\Delta H}{\tan\theta(t)}+\frac{\delta_{\mathrm{k}}-\delta_{\theta^{\wedge}}+\Delta x}{2}\right)^2+(\Delta H)^2>r_{\mathrm{d}}^2 \tag{15}$$

where $\delta_{\theta^{\wedge}}$ is the shrinkage thickness under the condition of conservative estimation of the rock displacement angle, and Δx is the horizontal disturbance difference at different rock movement angles, so there is

$$\Delta x=\Delta H\left(\frac{1}{\tan\theta^{\wedge}}-\frac{1}{\tan\theta(t_0)}\right) \tag{16}$$

δ_{k} has been computed. For the effective cumulative thickness of approximately parallel ore belts, the weight ratio can be determined:

$$\delta_{\mathrm{k}}=\sum_{i=1}^{n}\delta_i \tag{17}$$

where δ_i is the average thickness of ore belt i, and n is the number of ore belts.

Formulas (16) and (17) are substituted into Formula (15). Simultaneously, let $\theta(t_0)=\theta_0$, $\theta(t)=\theta$; we perform the square and simple transformation, and the more general judgment formula can be obtained:

$$\frac{\Delta H}{\tan\theta}+\frac{\sum_{i=1}^{n}\delta_i-\delta_{\theta^{\wedge}}}{2}+\frac{1}{2}\Delta H\left(\frac{1}{\tan\theta_{\mathrm{s}}}-\frac{1}{\tan\theta_0}\right)>\sqrt{r_{\mathrm{d}}^2-(\Delta H)^2} \tag{18}$$

where θ_{s} is the rock displacement angle selected according to experience.

To facilitate calculation and understanding, a simple substitution transformation is performed so that the left side of Formula (18) is equal to x_{r}. Obviously, under the condition of determining the parameters and mean elevation of the predicted formula, the right side of Formula (18) is a constant, and let it be M. Thus, formula (18) is expressed as

$$x_{\mathrm{r}}>M \tag{19}$$

where x_{r} is the horizontal perturbation distance of different moving angles; M is the lower limit of plane safety distance for complete mining at z level.

The criterion for successfully transforming the three-dimensional safety distance into two-dimensional state has the advantages of simplicity and strong applicability, and brings convenience to the advance prediction of the influence range of underground mining on the surface.

2.5 Application of correction formula and criterion

2.5.1 Application of rock movement angle selection in Jianshan Iron Mine

The Jianshan Underground Mine in Panzhihua Iron Mine (Jianshan Iron Mine) is an important source of iron ore in Panzhihua Iron and Steel Group. The upper wall rock of the Jianshan Iron Mine is mainly iron-bearing gabbro. There are five ore belts in the mining area, of which IV is scattered, and V−VIII appear approximately parallel in the vertical direction with large thicknesses. The ore body strikes from east to west with an inclination of 55°.

The mine has a road near the surface above the ore body, which is a traffic lane in Renhe District of Panzhihua City and needs key protection. To ensure highway safety, the problem of how to mine more ore is urgent to solve.

(1) Acquisition of correction factors

Based on the definition of rock strength on the correction factor, some mechanical parameters were required. Therefore, uniaxial compression and Brazilian splitting experiments on the rock samples drilled in the mine were performed. Through uniaxial compression test, the mechanical parameters of iron-bearing gabbro can be obtained, as shown in Table 1.

The tensile strength of iron-bearing gabbro can

Table 1 Uniaxial compressive test results of iron-bearing gabbro

Sample No.	D/ mm	L/ mm	Uniaxial compressive strength, σ_{c}/MPa		Elastic modulus, E_{e}/GPa		Poisson ratio, v	
			Actual measurement	Mean value	Actual measurement	Mean value	Actual measurement	Mean value
D1	49.68	100.34	190.186	197.04	76.125	76.77	0.20	0.22
D2	49.73	100.56	219.659		77.966		0.22	
D3	49.83	100.33	181.061		76.608		0.23	
D4	49.76	100.72	197.245		76.372		0.23	

D and L are the diameter and axial length of the rock specimen, respectively

be obtained through the Brazilian splitting test. The results are shown in Table 2.

Table 2 Brazilian splitting test results of iron bearing gabbro

Sample No.	D/ mm	L/ mm	Peak load, P/kN	Uniaxial tensile strength, σ_t/MPa	
				Actual measurement	Mean value
DL1	49.78	25.89	21.601	11.00	12.16
DL2	49.60	25.92	23.204	11.82	
DL3	49.99	25.91	21.640	11.02	
DL4	49.68	25.72	29.036	14.79	

The designed sectional height of the mine is 20 m. When the height of the ore drawing layer is 20 m, the height of the loose ellipsoid and the maximum radius of the discharge funnel are 54.99 and 9.60 m, respectively.

(2) Calculation of highway mean elevation

This study focuses on the influence of underground mining on the corner of the road heading northeastward. The mean elevation at the corner of the highway is required in subsequent theoretical calculations. The points are randomly marked (unequal density) according to the weight, and the range of points is 3 times greater than the turning radius of the highway.

Distinguishing the equidistant point, treating the point density differently, and allocating the artificial weight yield:

$$H_G=\sum_{i=1}^{n}\varsigma_i H_i \tag{20}$$

where ς_i is the manually set weight coefficient of each section, and H_i is the expected elevation of all sample points in each section.

The elevation of 21 points is obtained in the three-dimensional model, which is divided into left, middle and right sections. Because of nonuniform points, the average weight is obtained firstly. The minimum mining level of the mine is +900 m, and the allowable relative error of elevation calculation is 0.0358, so the elevation weight of the important turning radius area is 0.36, and the weight coefficient of the influence of the two wings is 0.32. Then, the average elevation of the road corner is +1678.93 m. The mine has been mined to the level of +1300 m, so the height difference of the disturbed lead hammer is 378.93 m.

(3) Security verification of different moving angle schemes

According to the design scheme of the original security pillar, the thickness of the reserved security pillar at the 60° movement angle is 49.23 m, i.e., $\delta_{60°}$, as mentioned in Section 2.4. According to the geological exploration data of the mine, the geometric parameter information of the four ore zones can be obtained, as shown in Table 3 (The thickness of ore belt IV is extremely thin, and its contribution to the overall thickness is negligible), as shown in Table 3.

To verify the feasibility of optimizing the range of security pillars by increasing the rock movement angle, 60°, 61°, 62°, 63°, 64° and 65° were used as alternative rock movement angles, and the selected rock movement angles have the greatest disturbance impact under their respective working conditions. The safety prediction was performed using Formula (19). After substituting the data into the above formula, the judgment results are shown in Table 4.

Through the modified formula and two-dimensional safety criterion, it can be concluded that the maximum rock movement angle can be taken as 64° only considering the road corner in the northeast direction, which best optimizes the range of security pillars and improves the ore recovery rate.

Table 3 Main geometric parameters of Jianshan ore belt

Geometric parameter	Ore belt code			
	V	VI	VII	VIII
Minimum thickness/m	24.94	−	32.41	19.04
Maximum thickness/m	56.56	−	86.65	49.78
Average thickness/m	42.05	51.77	59.27	34.53
Thickness stability	Stable	Stable	Relatively stable	Relatively stable

Table 4 Safety evaluation of rock movement angle based on two-dimensional safety criterion

Rock movement angle/(°)	Two-dimensional criterion parameter			
	x_r/m	M/m	Criterion relationship (Yes/No)	Safety (Yes/No)
60	287.97	267.78	Yes	Yes
61	283.61	267.78	Yes	Yes
62	279.32	267.78	Yes	Yes
63	273.59	267.78	Yes	Yes
64	270.99	267.78	Yes	Yes
65	266.94	267.78	No	No

2.5.2 Application of mining disturbance range prediction by caving method

The mining disturbance ranges of the Dahongshan Iron Mine, Chengchao Iron Mine, Shizishan Copper Mine, Jinshandian Iron Mine, Xishimen Iron Mine and Gongchangling Iron Mine are predicted by the new modified formula. Field monitoring data of these six mines in different periods were also collected. The prediction results are shown in Table 5.

Table 5 Prediction results of disturbance range of 6 caving mines

Name of mine	Date	Measured value/m	Predicted value/m	Relative error/%
Dahongshan Iron Mine	Dec., 2020	498	499	0.20
Chengchao Iron Mine	May, 2020	538	540	0.37
Shizishan Copper Mine	Sept., 2015	425	432	1.65
Jinshandian Iron Mine	Feb., 2019	405	408	0.74
Xishimen Iron Mine	Dec., 2014	300	299	0.33
Gongchangling Iron Mine	July, 2017	270	279	3.33

Generally, the pros and cons of the prediction model can be tested according to the posteriori error method, and the test indices are the posteriori error ratio and small probability error. According to the posteriori error test theory and Table 5, it is calculated that the posteriori error ratio is 0.0357, and the small probability error is greater than 0.95 [36]. In the posteriori error method test, when the posterior ratio is 0.35 and the small probability error is greater than 0.95, the prediction effect of the model is excellent, so the prediction accuracy of the new method is high.

3 Numerical simulation based on FLAC^{3D} model

Most studies show that the simulation results of surface subsidence based on FLAC^{3D} basically agree with the actual situation [12,37,38]. Since the selection of the moving angle of the Jianshan Iron Mine is a scheme study and the field monitoring data cannot be obtained, FLAC^{3D} model was used to simulate the mining to verify the reliability of the new method in Jianshan Iron Mine.

3.1 Establishment of model

To simulate the mining process, rock movement angles of 60°, 61°, 62°, 63°, 64° and 65° were also selected as five independent working conditions. Parameter reduction of rock and soil mass is a necessary method to ensure the reliability of finite element simulation results [39]. The mechanical parameters assigned to each group in the mine model were reduced based on the Hoek−Brown strength criterion in RocData. The reduced mechanical parameters are shown in Table 6.

To ensure the accuracy of simulating the impact of excavation, the influence area of the underground pit was determined to be 3−5 times its excavation range according to Saint−Venant's principle [40]. The numerical model was built to simulate the excavation affected zone with three times the size of the open pit in the length and width directions. Taking the model of 60° rock movement angle of the security pillar as an example, the model length is 4038 m, the width is 3783 m, and the height is 1594 m. The boundary constraint of the model adopts displacement constraint. Due to the limited mining range, the rock mass displacement far away from the stope is very small, so the boundary model displacement can be regarded as 0. The model is constrained by X-, Y- and Z-directions, respectively. The left and right (X-direction) boundary, the front and rear (Y-direction) boundary and the bottom (Z-direction) boundary of the model are subjected to displacement constraints, and the upper boundary is a free boundary. The numerical model can be mainly divided into the

Table 6 Mechanical parameters of FLAC^{3D} model for rock masses

Mechanical parameter	Rock type				
	Fe1	Fe2	Fe3	Ferrogabbro	Marble
Tensile strength/MPa	0.027	0.046	0.052	0.154	0.308
Elastic modulus/GPa	3.786	5.048	5.046	10.001	10.001
Poisson ratio	0.270	0.280	0.260	0.220	0.260
Angle of internal friction/(°)	34.260	38.350	40.390	49.200	37.790
Density/(g·cm^{-3})	4.420	4.020	3.510	3.150	2.870
Bulk modulus/GPa	2.743	3.824	3.504	5.953	6.945
Shear modulus/GPa	1.491	1.972	2.002	4.099	3.969

upper wall rock, lower wall rock, ore body, and open pit. The solid model of 60° rock movement angle is shown in Fig. 2.

The ore body is subdivided into five ore zones. The ore zone is excavated to the 1300 m level. The surface and curved surface formed by the influence line at the 1300 m level are determined according to the rock movement angle, and the ore body is divided into a security pillar and a mining area (Fig. 3).

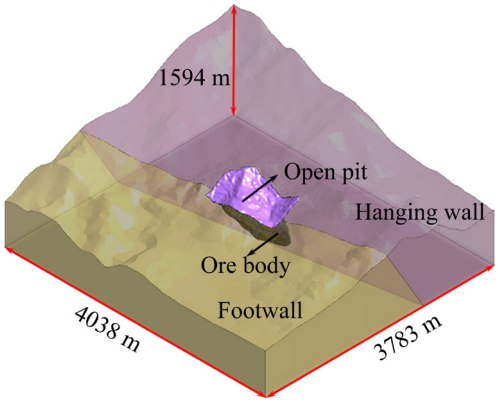

Fig. 2 Solid model of 60° rock movement angle

Since the corner of the highway is near the open pit slope, the exposed sky slope is an ultra-high and steep slope, and the corner cannot be simply monitored according to relevant standards of the highway. The research is performed here according to the relevant railway standards. According to the railway safety management regulations, the protected area of high-speed railways is 20 m away from the outside of the railway. Therefore, in this study, monitoring points are set at the position extending 20 m away from the highway to monitor the impact of mining at different moving angles on the surface highway.

According to TB 10001—2016, the post-construction settlement control limit of the transition section of the high-speed railway subgrade is 50 mm [41]. Therefore, in the numerical simulation of the mine, when the displacement subsidence or floor heave exceeds 50 mm, the determined rock engineering structure may be unstable.

3.2 Analysis of calculation results

To analyze the influence of mining at different strata movement angles on surface roads, the excavation process is divided into the initial stage (mining zone VIII), the middle stage (mining zone VI) and the late stage (mining zone IV), among which the mining range in the late stage is the largest and most significant mining influence period. Each period is used as an excavation step for the simulation calculation. The direction near the slope of the open pit is the direction most likely to cause failure of the rock and soil mass, which is defined as the *Y*-direction in the model. Therefore, the maximum tensile stress, plastic zone and displacement cloud map in the *Y*-direction of the same monitoring point in the mine at different angles in the late stage of excavation are obtained. The cloud pattern of each angle is the same, and there are differences in values. Therefore, only the cloud pattern and *Y*-direction displacement curve at the late stage of excavation with a rock displacement angle of 60° are given in Fig. 4.

Figures 4(a) and (b) show that in the late stage of mining, the iron-bearing gabbro in the hanging wall is mainly characterized by tensile stress, and the peak value of tensile stress is much greater than the reduced tensile strength of iron-bearing gabbro. The tensile failure is further expanded, and the

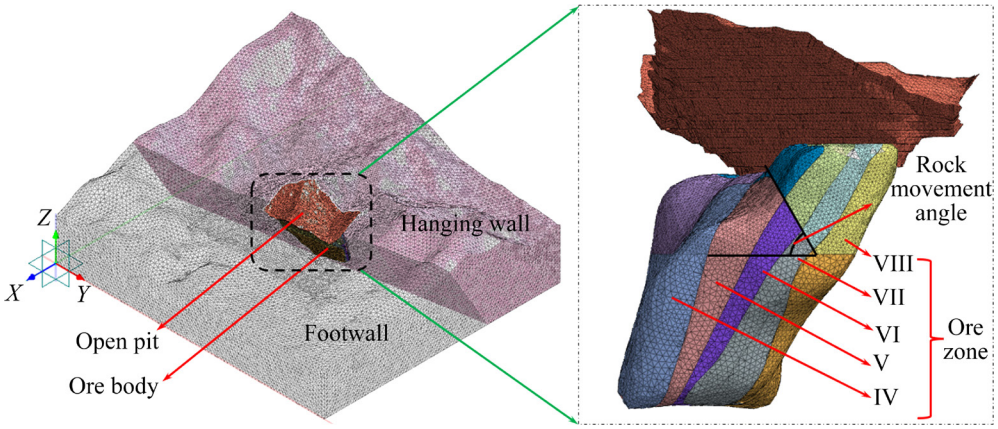

Fig. 3 Mesh refinement grouping for 60° model

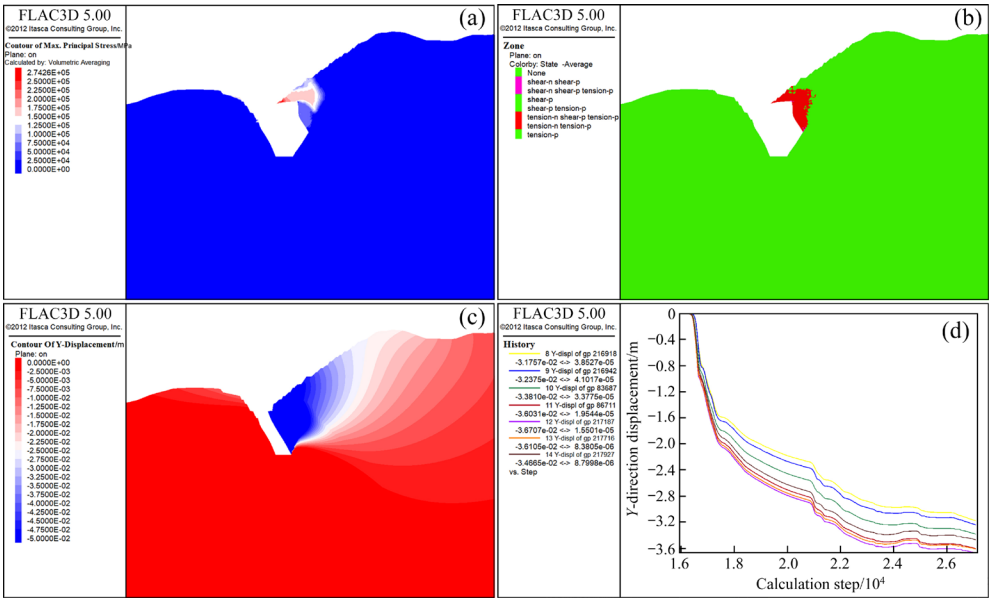

Fig. 4 Results of late excavation at 60° rock shift angle: (a) Maximum principal stress; (b) Plastic zone; (c) *Y*-direction displacement cloud map; (d) *Y*-direction displacement

plastic zone is basically penetrated, but the protective belt of the highway has not been affected. Figures 4(c) and (d) show that the *Y*-direction has negative displacement, and the direction is vertical to the north of the ore body trend. Simultaneously, the *Y*-direction displacement shows a trend of first rapidly increasing and subsequently slowly increasing.

The displacement of 6 rock displacement angles in the *Y*-direction gradually increases with the excavation progress, which is consistent with the actual situation. The variation law between the maximum displacement in this direction and the number of excavation steps is shown in Fig. 5. In Fig. 5, 1, 2 and 3 correspond to the initial, middle

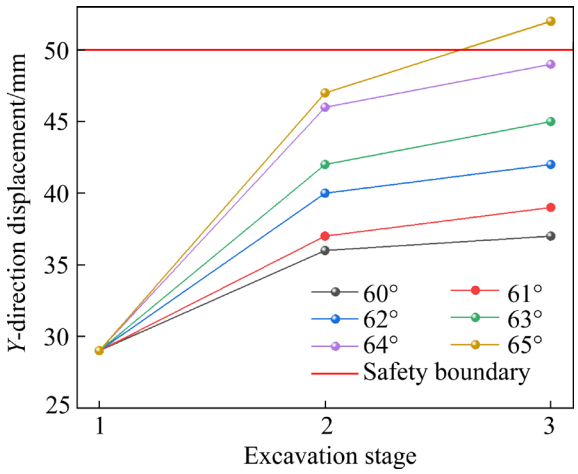

Fig. 5 Relationship between displacement peak in *Y*-direction and excavation stage

and late excavation stages of the entire ore body, respectively. The figure shows that in the late excavation with a rock displacement angle of 65°, the displacement in the *Y*-direction is greater than the control limit value.

The peak tensile stress curves of different angles and excavation stages are obtained through simulation, as shown in Fig. 6. As shown in Fig. 6, the "0" in the transverse coordinate indicates that the mining stage has not started. In this figure, when the same rock displacement angle is taken, the peak tensile stress at the early stage of excavation is the largest; then, it rapidly decreases; finally, it slowly decreases. The peak tensile stress at all excavation stages is greater than the tensile strength. The peak law of tensile stress is similar to the strength curve of a rock mass, which proves that the self-similarity of fractal theory is applicable to the study of rock masses.

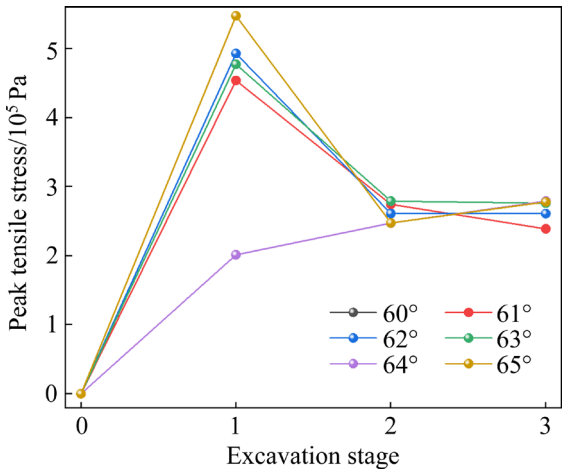

Fig. 6 Relationship between maximum tensile stress and excavation stage

From the simulation results of these six angles, it can be concluded that when the rock movement angle is 65°, the displacement in the *Y*-direction is greater than the control limit value, so the working condition with a rock movement angle of 65° affects the safety of the highway. Therefore, to protect the highway, the maximum rock movement angle of the mine is 64°. Through numerical simulation, the correctness of the correction formula based on mechanical parameters in Jianshan Iron Mine is verified.

For the Jianshan Underground Iron Mine, the modified formula and numerical simulation have the same conclusion, but it is necessary to verify whether different methods will produce singular phenomena (the degree of influence of the method on the results). Therefore, it is necessary to conduct contingency table analysis on the two methods.

4 Contingency table analysis of two methods

4.1 Contingency table theory

The contingency table is a frequency table listed by the cross-analysis of the observed data with two or more attributes. Here, the contingency table with the measurement of $c\times w$ is taken as an example for the cross-analysis of the data correlation degree [42]. Table 7 shows a contingency table that verifies the correlation between methods and results.

Table 7 Contingency table model for verifying method security

Method	Result				Total number
	x_1	x_2	⋯	x_w	
y_1	f_{11}	f_{12}	⋯	f_{1w}	r_1
y_2	f_{21}	f_{22}	⋯	f_{2w}	r_2
⋮	⋮	⋮	⋯	⋮	⋮
y_c	f_{c1}	f_{c2}	⋯	f_{cw}	r_w
Total number	s_1	s_2	⋯	s_w	n

In Table 7, the total count of row (column) observation values constitutes the row (column) edge distribution, and the calculation formula of the total count is as follows:

$$\begin{cases} r_k = \sum_{j=1}^{w} f_{kj}, \ 1 \le k \le c \\ s_l = \sum_{i=1}^{c} f_{il}, \ 1 \le l \le w \end{cases} \tag{21}$$

Based on the edge distribution generated by the contingency table, an expected frequency matrix can be obtained:

$$\boldsymbol{E} = \begin{bmatrix} e_{11} & e_{12} & \cdots & e_{1w} \\ e_{21} & e_{22} & \cdots & e_{2w} \\ \vdots & \vdots & & \vdots \\ e_{c1} & e_{c2} & \cdots & e_{cw} \end{bmatrix} \tag{22}$$

If x and y are independent of each other, the probability and expected frequency of an actual frequency falling on i rows and j columns can

be calculated according to the probability multiplication formula.

$$e_{ij}=\frac{r_i s_j}{n} \tag{23}$$

where f_{ij} is the actual frequency; r_i is the total of row i; s_j is the total of column j; n is the sum of all data; e_{ij} is the expected frequency.

To test the independence between multiple variables, the Pearson χ^2, a statistic with degrees of freedom $(c-1)(w-1)$, is introduced, and its calculation formula is

$$\chi^2=\sum_{i=1}^{c}\sum_{j=1}^{w}\frac{(f_{ij}-e_{ij})^2}{e_{ij}} \tag{24}$$

Based on the Pearson consistent test statistics, the more suitable correlation coefficients for contingency tables are obtained. There are three commonly used measurement coefficients, which have their own use conditions. The numbers of rows and columns of the contingency table formed in this study are obviously unequal. Therefore, the v coefficient is used as the measurement index to cross-analyze the correctness of the method. The coefficient v is defined as

$$v=\sqrt{\frac{\chi^2}{n\min\left[(c-1),(w-1)\right]}} \tag{25}$$

4.2 Analysis of security retention rate based on continuity table

Both methods give the upper limit value of safety, and there is a difference between the index given by each angle and the limit value of the corresponding index. Therefore, to verify the impact of the two methods on the correctness of the rock movement angle results (mainly verify whether different methods will change the safety degree of different angles), the safety retention rate is introduced, and its calculation formula is as follows:

$$\vartheta=\frac{|u-u_\theta|}{u} \tag{26}$$

where ϑ is the security retention rate; u is the safety upper limit that corresponds to the two methods; u_θ is the corresponding calculated value under each angle working condition.

Assuming that matrix $\boldsymbol{B}$ obtains a new matrix through finite elementary transformation, the two matrices before and after transformation are equivalent matrices, so $\boldsymbol{B}\sim k\boldsymbol{B}$. If the contingency table only retains all actual frequencies, it can form a matrix [43]. Therefore, for the convenience of research, the retention rate of each unit is multiplied by 1000, and the value at this time is called the safe space. For the mine, the relevant data of the safe rock movement angle are obtained, and the contingency table in Table 8 is generated.

Table 8 Column data in secure space for two methods

Method	Rock movement angle/(°)					Total number
	60	61	62	63	64	
Correction formula	75	59	42	22	12	211
FLAC^{3D} model	260	220	160	100	20	760
Total number	335	279	202	122	32	971

The data in Table 8 are substituted into Formula (22) and Formula (23) to obtain the expected frequency matrix. The v factor calculated by Formula (25) is 0.078, which proves that the new method does not significantly affect the security. Therefore, the new method predicts that the disturbance range of underground mining on the surface is applicable.

Compared with FLAC^{3D} model and some existing prediction methods, the new method has certain advantages in cost and operation difficulty, and it is more convenient for mine engineers to apply. Therefore, the new method has a broad application prospect in mining collapse prediction, and we will also apply the new method to more metal caving mines.

5 Conclusions

(1) A new method to predict the mining disturbance range of metal mines based on mechanical parameters is established, and the disturbance safety criterion is derived based on the equivalent disturbance center and disturbance attenuation sphere.

(2) In the comparison of the predicted value and measured value, the posterior error ratio is 0.0357. The correlation coefficient between the Johanshan prediction results and FLAC^{3D} simulation results is only 0.078. Therefore, the new method has high prediction accuracy and no significant influence on the safety degree.

(3) The new method is based on some ideal assumptions and is the first attempt of the multi-boundary constraint parameter adjustment theory, which requires further study.

Acknowledgments

The authors are grateful for the financial supports from the National Natural Science Foundation of China (No. 52104109), and the National Key Research and Development Program of China (No. 2020YFC1909801).

References

[1] WANG Shao-feng, SUN Li-cheng, HUANG Lin-qi, SHI Ying, YAO Jin-rui, DU Shao-lun. Non-explosive mining and waste utilization for achieving green mining in underground hard rock mine in China [J]. Transactions of Nonferrous Metals Society of China, 2019, 29(9): 1914−1928.

[2] LI Peng, CAI Mei-feng. Challenges and new insights for exploitation of deep underground metal mineral resources [J]. Transactions of Nonferrous Metals Society of China, 2021, 31(11): 3478−3505.

[3] DING Kuo, SONG Gao-feng, LI Hui. Study on monitoring, statistics, movement and deformation law of mine subsidence [J]. Geotechnical and Geological Engineering, 2020, 38(6): 6207−6219.

[4] CHEN Gang, WANG Qiong, LI Xiao-ming. Prediction of surface subsidence due to mining [J]. Integrated Ferroelectrics, 2020, 209(1): 76−85.

[5] ORWAT J. Mining terrain curvatures approximation using the polynomials and a subsidence trough profile fragmentation [J]. Journal of Physics: Conference Series, 2021, 1781(1): 012014.

[6] KAMILA P F, ANDRZE J B. Monitoring mining-induced subsidence by integrating differential radar interferometry and persistent scatterer techniques [J]. European Journal of Remote Sensing, 2021, 54(S1): 18−30.

[7] HE Qian, ZHANG Yong-hong, WU Hong-an, LUO Yong. Mining subsidence monitoring with modified time-series SAR interferometry method based on the multi-level processing strategy [J]. IEEE Access, 2021, 9: 106039−106048.

[8] XU Xiao-bo, MA Chao, LIAN Da-jun, ZHAO De-zheng. Inversion and analysis of mining subsidence by integrating DInSAR, offset tracking, and PIM technology [J]. Journal of Sensors, 2020, 2020: 1−15.

[9] JIANG Chuang, WANG Lei, YU Xue-xiang, CHI Shen-shen, WEI Tao, GUO Zhong-chen. A DPIM-InSAR method for monitoring mining subsidence based on deformation information of the working face after mining has ended [J]. International Journal of Remote Sensing, 2021, 42(16): 6330−6358.

[10] WANG Guo-rui, WU Qiang, LI Pei-xian, CUI Xi-min, GONG Yong-feng, ZHANG Jia, TANG Wei. Mining subsidence prediction parameter inversion by combining GNSS and DInSAR deformation measurements [J]. IEEE Access, 2021, 9: 89043−89054.

[11] ZHAO Xing-dong, ZHU Qian-kun. Analysis of the surface subsidence induced by sublevel caving based on GPS monitoring and numerical simulation [J]. Natural Hazards, 2020, 103(3): 3063−3083.

[12] WANG Ping. Study of subsidence angle and its area range of Xiaoguanzhuang Iron Mine [D]. Shenyang: Northeast University, 2015. (in Chinese)

[13] LI Jing-yu, WANG Lei. Mining subsidence monitoring model based on BPM-EKTF and TLS and its application in building mining damage assessment [J]. Environmental Earth Sciences, 2021, 80(11): 396.

[14] YUAN De-bao, GENG Cheng-xing, ZHANG Ling, ZHANG Zhen-chao. Application of Gray-Markov model to land subsidence monitoring of a mining area [J]. IEEE Access, 2021, 9: 118716−118725.

[15] KIM Y, LEE S S. Application of artificial neural networks in assessing mining subsidence risk [J]. Applied Sciences, 2020, 10(4): 1302.

[16] CHEN Qiu-ji, LI Ji-ye, HOU En-ke. Dynamic simulation for the process of mining subsidence based on cellular automata model [J]. Open Geosciences, 2020, 12(1): 832−839.

[17] CHI Shen-shen, WANG Lei, YU Xue-xiang, FANG Xin-jian, JIANG Chuang. Research on prediction model of mining subsidence in thick unconsolidated layer mining area [J]. IEEE Access, 2021, 9: 23996−24010.

[18] JIANG Yue, MISA R, LI Peng-yu, YUAN Xin, SROKA A, JIANG Yan. Summary and development of mining subsidence theory [J]. Metal Mine, 2019(10): 1−7. (in Chinese)

[19] LIU Zhi-xiang, HAN Ke-wen, YANG Shan, LIU Yu-xi. Fractal evolution mechanism of rock fracture in undersea metal mining [J]. Journal of Central South University, 2020, 27(4): 1320−1333.

[20] BENOIT B. Fractals: Form, chance, and dimension [M]. New York: W. H. Freeman, 1977.

[21] CHEN Lu-wang, LI Rui-rui, WANG Lan-ting, ZHANG Jie, OU Qing-hua, REN Xing-xing, ZHOU Kan-dong. Microfracture development and chemical damage analysis of limestone based on fractal theory [J]. Quarterly Journal of Engineering Geology and Hydrogeology, 2021, 54(3): 1−8.

[22] YUAN Jie, LIU Zhu-hui, WU Xun, LI Ya-dong. Calculation formula and process optimization research of random medium method to predict the surface subsidence and deformation [J]. Electronic Journal of Geotechnical Engineering, 2016, 21: 4133−4141.

[23] WU Fa-quan, WU Jie, HAN Bao, LI Bo, SHAN Zhi-gang, KONG De-heng. Advances in statistical mechanics of rock masses and its engineering applications [J]. Journal of Rock Mechanics and Geotechnical Engineering, 2021, 13(1): 22−45.

[24] ZELENTSOV V B, LAPINA P A, MITRIN B I, EREMEYEV V A. Characterization of the functionally graded shear modulus of a half-space [J]. Mathematics, 2020, 8(4): 640.

[25] CAO Zheng-zheng, DU Feng, XU Ping, LIN Hai-xiao, XUE Yi, ZHOU Yue-jin. Control mechanism of surface subsidence and overburden movement in backfilling mining based on laminated plate theory [J]. Computers, Materials and

Continua, 2017, 53(3): 175−186.
[26] HOEK E, BROWNE T, ASCE M. Empirical strength criterion for rock masses [J]. Journal of the Geotechnical Engineering Division, 1980, 106(9): 1013−1035.
[27] LEMOS N A, MORICONI M. On the consistency of the Lagrange multiplier method in classical mechanics [J]. American Journal of Physics, 2021, 89(8): 776−782.
[28] HAESER G, HINDER O, YE Yin-yu. On the behavior of Lagrange multipliers in convex and nonconvex infeasible interior point methods [J]. Mathematical Programming, 2021, 186(1/2): 257−288.
[29] VAHID M, ABBAS M. Directional rock mass rating (DRMR) for anisotropic rock mass characterization [J]. Bulletin of Engineering Geology and the Environment, 2021, 80(6): 4471−4499.
[30] SI Xue-feng, HUANG Lin-qi, LI Xi-bing, GONG Feng-qiang, LIU Xi-ling. Mechanical properties and rockburst proneness of phyllite under uniaxial compression [J]. Transactions of Nonferrous Metals Society of China, 2021, 31(12): 3862−3878.
[31] SCHWARZHANS E, LOCK M, ERKER P, FRIIS N, HUBER M. Autonomous temporal probability concentration: Clockworks and the second law of thermodynamics [J]. Physical Review X, 2021, 11(1): 011046.
[32] LUO Zhou-quan, WANG Wei, QIN Ya-guang, XIANG Jun. Early warning of rock mass instability based on multi-field coupling analysis and microseismic monitoring [J]. Transactions of Nonferrous Metals Society of China, 2019, 29(6): 1285−1293.
[33] HU Jian-hua, YANG Dong-jie. Meso-damage evolution and mechanical characteristics of low-porosity sedimentary rocks under uniaxial compression [J]. Transactions of Nonferrous Metals Society of China, 2020, 30(4): 1071−1077.
[34] WANG Pin, YIN Tu-bing, HU Bi-wei. Dynamic tensile strength and failure mechanisms of thermally treated sandstone under dry and water-saturated conditions [J]. Transactions of Nonferrous Metals Society of China, 2020, 30(8): 2217−2238.
[35] SHEN Qing-qing, RAO Qiu-hua, LI Zhuo, YI Wei, SUN Dong-liang. Interacting mechanism and initiation prediction of multiple cracks [J]. Transactions of Nonferrous Metals Society of China, 2021, 31(3): 779−791.
[36] MENG Yan, HUANG Jian-ming, LEI Ming-tang, LI Yu, HUANG Jian-ling. Quantitative forecast method of karst collapse based on grey Verhulst model [J]. Carsologica Sinica, 2009, 28(1): 17−22. (in Chinese)
[37] SUN Hong-jun, GAO Er-chong, ZHOU Ai-peng. Numerical simulation of uneven settlement of municipal solid waste landfill by FLAC3D [J]. Waste Management & Research, 2022, 40(4): 374−382.
[38] ZHOU Hong-sheng, WANG Yun-sheng, SHEN Tong, FENG Qian-qian. The comprehensive treatment of the ancient landslide deformable body in the giant deep rock bedding based on the FLAC analysis model [J]. Earth Sciences Research Journal, 2019, 23(4): 303−308.
[39] AN Xiao-fan, LI Ning. Non-equal strength reduction analysis of soil slopes considering progressive failure [J]. Soil Mechanics and Foundation Engineering, 2021, 58(4): 273−279.
[40] CHAUDHURI R A, XIE Min-sheng. On three-dimensional asymptotic solution, and applicability of Saint−Venant's principle to pie-shaped wedge and end face (of a semi-infinite plate) boundary value problems [J]. Engineering Fracture Mechanics, 2015, 142: 93−107.
[41] TB 10001—2016. Code for design of railway subgrade [S]. (in Chinese)
[42] GOLD S, WHITE E, ROEDER W, MCALEENAN M, KABBAN C S, AHNER D. Probabilistic contingency tables: An improvement to verify probability forecasts [J]. Weather and Forecasting, 2020, 35(2): 609−621.
[43] WANG Ming-hui, YUE Ling-ling, LIU Qiao-hua. Elementary transformation and its applications for split quaternion matrices [J]. Advances in Applied Clifford Algebras, 2020, 30(1): 1−10.

金属矿崩落法扰动范围预测新方法及应用

周科平[1]，李 亮[1]，林 允[1]，熊 信[1]，杨念哥[1]，陈树林[2]

1. 中南大学 资源与安全工程学院，长沙 410083；
2. 攀钢矿业有限责任公司 攀枝花铁矿，攀枝花 617025

摘 要：为量化金属矿崩落法扰动范围，提出一种基于岩石力学参数扰动范围的预测新方法。通过将岩石力学指标与随机介质理论相结合，建立扰动范围预计修正公式。基于扰动等效中心和扰动衰减球面，推导金属矿山开采扰动的二维安全判据。将该方法应用于 6 个矿山和尖山矿，并利用 FLAC^{3D} 模型对尖山矿进行数值模拟。经对比，预测值与实测值的后验差比值为 0.0357，多因素交叉分析得到该方法对结果产生的相对误差仅为 0.078。研究表明，该方法的预测精度高，且不会对安全性产生显著影响。

关键词：扰动范围；修正公式；二维安全判据；数值模拟；多因素交叉分析

(Edited by Wei-ping CHEN)